Supporting Information

The Organophosphine Oxide Redox Shuttle Additive That Delivers Long-term Overcharge Protection in 4 V Lithium-ion Batteries

Jinhua Huang [ab‖], Nasim Azimi[b‖], Lei Cheng[ac], Ilya A. Shkrob,[b] Zheng Xue,[b] Junjie Zhang[c], Nancy L. Dietz Rago[b], Larry A. Curtiss[ac], Khalil Amine[ab], Zhengcheng Zhang[ab]*, Lu Zhang[ab]*

[a]Joint Center for Energy Storage Research, [b] Chemical Sciences and Engineering Division, [c]Materials Science Division, Argonne National Laboratory, 9700 South Cass Avenue, Argonne, IL 60439-4837, USA

E-mail: zzhang@anl.gov; luzhang@anl.gov

***Materials*:** 1,4-dibromo-2,5-dimethoxybenzene (Sigma-Aldrich, 97%), 1, 4-difluoro-2,5-dimethoxybenzene (Alfa Aesar, 97%), *n*BuLi (Sigma-Aldrich, 2.5 M in hexanes), chlorodiisopropylphosphine (Sigma-Aldrich, 96%), *tert*-butyl hydroperoxide (Alfa Aesar, 70% aq. solution), sodium thiosulfate (Sigma-Aldrich, 99%), *N*, *N*-diisopropylamine (Sigma-Aldrich, ≥99%) were used as received. Gen 2 electrolyte (1.2 M $LiPF_6$ in 3:7 wt/wt mixture of ethylene carbonate and ethyl methyl carbonate) was purchased from Tomiyama High Purity Chemical Industries Ltd. LMO (D50 particle size: 10.7 μm) and MCMB (D50 particle size: 13-20 μm) active materials were provided by Cell, Analysis, Modeling and Prototyping (CAMP) facility at Argonne, which were purchased from Toda and Gelon, G15, respectively.

***Synthesis*:** BPDB and BPDFDB were synthesized according to the following procedures.

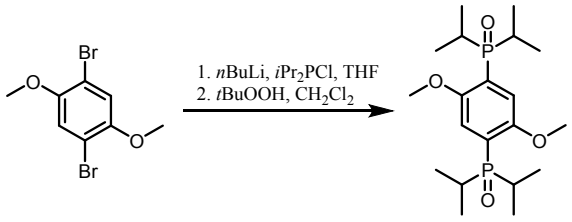

To a solution of 1,4-dibromo-2,5-dimethoxybenzene (2.0 g, 6.8 mmol) in Et_2O (100 mL) was added *n*BuLi (5.3 mL, 2.5 M in hexanes, 13.3 mmol) dropwise at -70 ºC under nitrogen. The mixture was allowed to warm to room temperature and stirred for 3 h before it was re-cooled to -70 ºC. Chlorodiisopropylphosphine (3.2 mL, 20.0 mmol) was

then added to the mixture, after which the solution was allowed to warm up to room temperature while stirring. The solvent was removed *in vacuo*, and the residue was dissolved in dichloromethane (50 mL) and filtered. The filtrate was treated with silica gel and stirred for 30 min. The solid was then filtered off and the filtrate was concentrated. The residue was dissolved in dichloromethane and treated with *tert*-butyl hydroperoxide (4.0 mL, 70% aq. solution, 28 mmol), and the mixture was stirred for another 3 h before it was quenched by saturated aqueous sodium thiosulfate. After stirring for 30 min, the reaction was partitioned between dicholoromethane and water. The organic phase was concentrated to provide a crude product, which was recrystallized from dichloromethane to afford pure BPDB (1.23 g, 45%) as a white solid. ^{1}H NMR (500 MHz, $CDCl_3$) δ 7.52 (dd, J = 11.6, 5.6 Hz, 2H), 3.86 (s, 6H), 2.46-2.39 (m, 2H), 1.25 (dd, J = 15.4, 7.1 Hz, 6H), 0.98 (dd, J = 16.7, 7.2 Hz, 6H); ^{13}C NMR (125 MHz, $CDCl_3$) δ 153.12 (dd, J = 10.8, 4.5 Hz), 123.86 (dd, J = 79.0, 1.5 Hz), 116.92 (dd, J = 7.4, 4.9 Hz), 55.77, 26.67 (d, J = 66.8 Hz), 16.64 (d, J = 2.7 Hz), 15.74 (d, J = 3.5 Hz). HRMS (EI$^+$): m/z calcd. for $C_{20}H_{37}O_4P_2$ $[M + H]^+$ 403.2162, found: 403.2166.

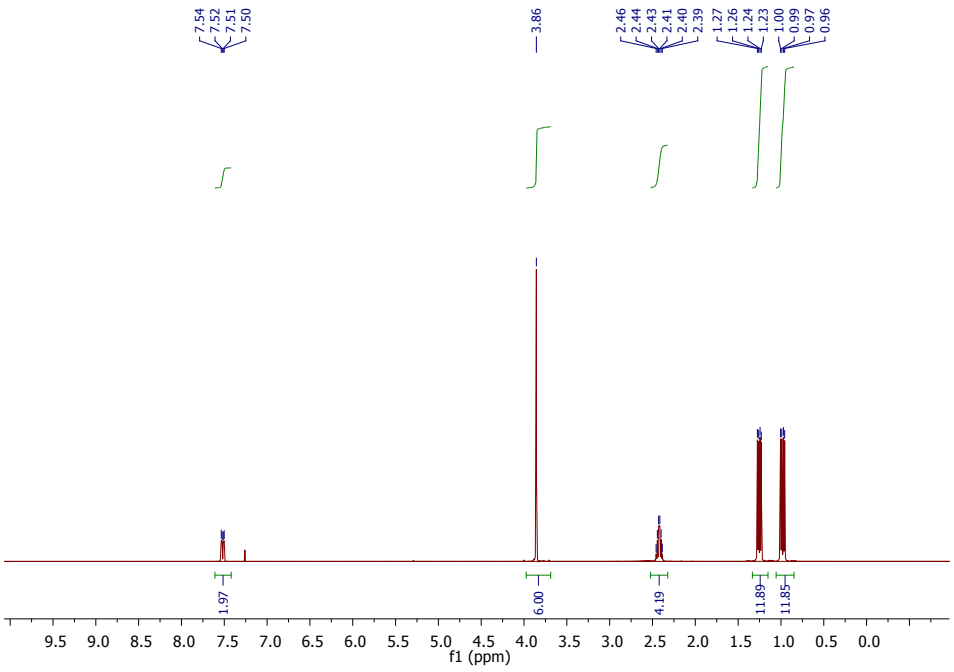

Figure S1. The ^{1}H NMR spectrum of BPDB in $CDCl_3$.

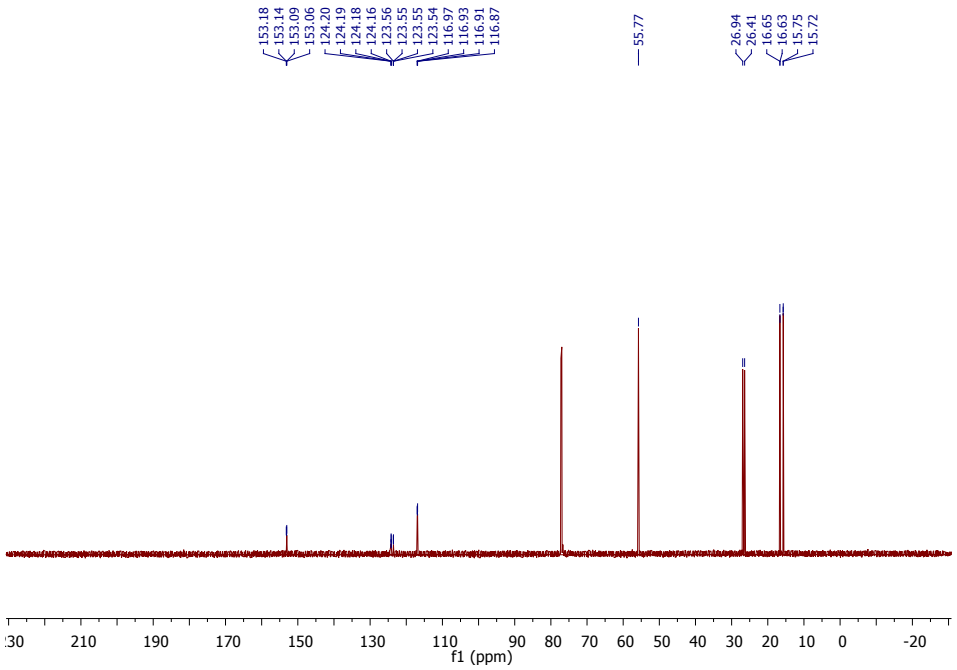

Figure S2. The ^{13}C NMR spectrum of BPDB in $CDCl_3$.

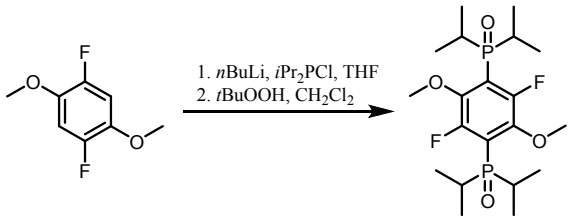

To a solution of *N*, *N*-diisopropylamine (4.5 mL, 31.5 mmol) in anhydrous THF (50 mL) was added *n*BuLi (12.6 mL, 2.5 M in hexanes, 31.5 mmol) dropwise at 0 °C under nitrogen. After 30 min, the solution was transferred into a cold solution (-95 °C) of 1, 4-difluoro-2,5-dimethoxybenzene (2.6 g, 15 mmol) in THF (250 mL). After stirring at -95 °C for 5 min, a solution of chlorodiisopropylphosphine (6.0 mL, 37.5 mmol) in THF (50 mL) was slowly added. The mixture was stirred at -95 °C for 1 h and then allowed to slowly warm up to room temperature while stirring for 12 h. The resulting solution was concentrated and the residue was dissolved in dichloromethane and filtered. To the filtrate, silica gel was added and the resulting mixture was stirred for 30 min. The silica gel was filtered off and the filtrate was concentrated. The residue was dissolved in dichloromethane (100 mL) and treated with *tert*-butyl hydroperoxide (8.2 mL, 70% aq. solution, 60 mmol), and the mixture was stirred for another 2 h before it was quenched by saturated aqueous sodium thiosulfate. After stirring for 30 min, the reaction was partitioned between dichloromethane and water. The organic phase was concentrated to provide a crude product, which was recrystallized from dichloromethane to afford pure

BPDFDB (4.08 g, 62%) as a white solid. ^{1}H NMR (500 MHz, $CDCl_3$) δ 3.95 (s, 6H), 2.44 (dq, *J* = 14.3, 7.1 Hz, 4H), 1.30 (dd, *J* = 16.3, 7.1 Hz, 12H), 1.14 (dd, *J* = 17.1, 7.2 Hz, 12H). ^{13}C NMR (125 MHz, $CDCl_3$) δ 152.31 (ddd, *J* = 251.9, 9.3, 3.8 Hz), 145.79-145.55 (m), 118.18 (ddd, *J* = 20.3, 15.2, 6.7 Hz), 62.58 (t, *J* = 3.0 Hz), 28.02 (d, *J* = 67.5 Hz), 16.55 (d, *J* = 2.7 Hz), 15.53 (d, *J* = 3.0 Hz); ^{19}F NMR (470 MHz, $CDCl_3$) δ -101.36. Molecular ion was not observed by GCMS due to low volatility of the compound. The chemical structure was confirmed by single crystal X-ray diffraction (cf. Figure S14).

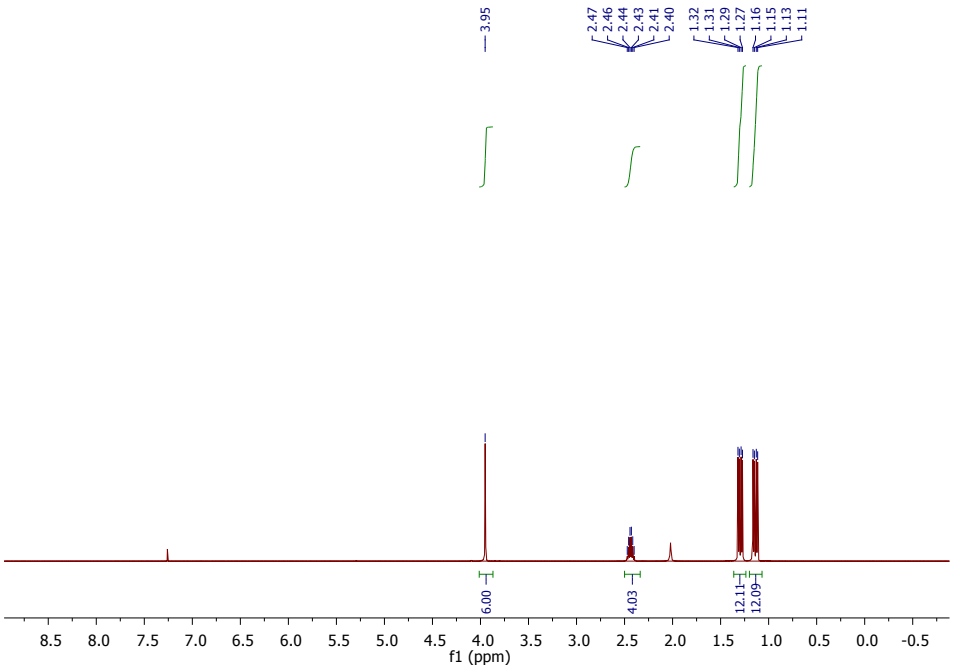

Figure S3. The ^{1}H NMR spectrum of BPDFDB in $CDCl_3$.

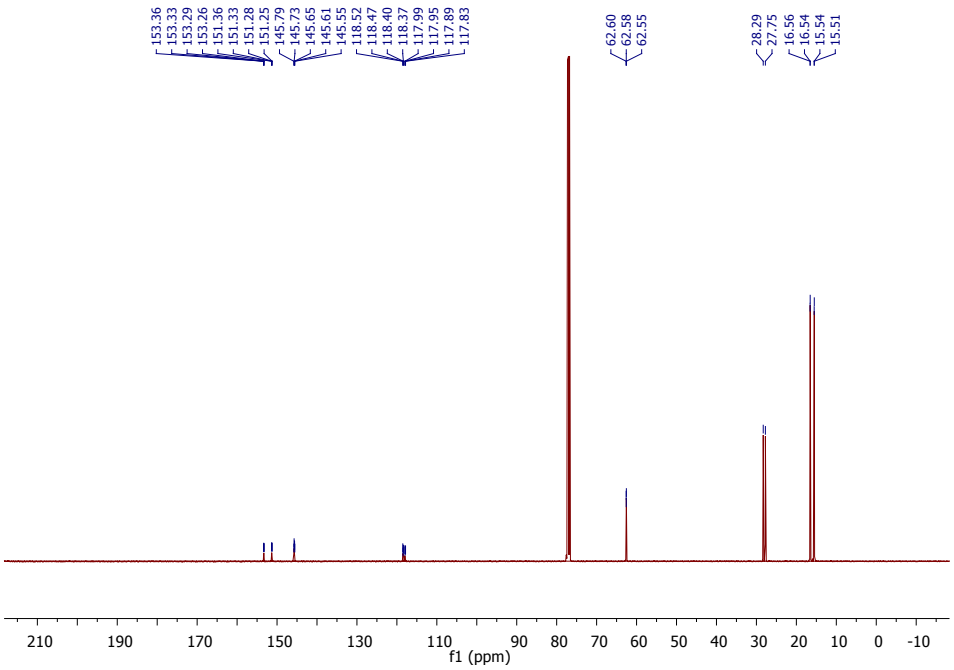

Figure S4. The ^{13}C NMR of BPDFDB in $CDCl_3$.

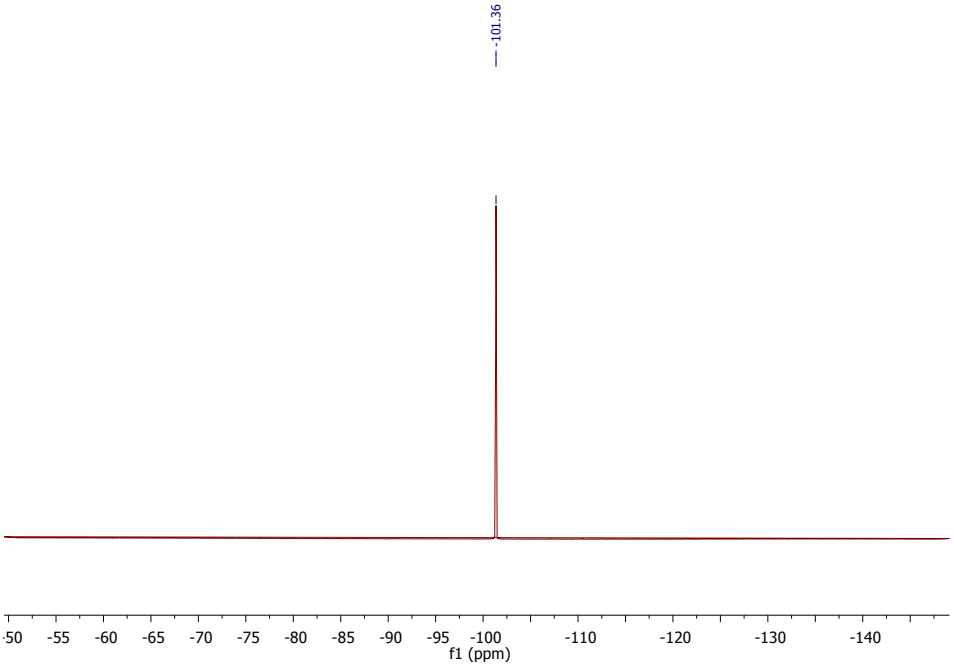

Figure S5. The ^{19}F NMR spectrum of BPDFDB in $CDCl_3$.

***Electrochemical measurements*:** Cyclic voltammetry (CV) experiments were performed in custom-made three electrode cells equipped with a 2 mm diameter Pt working electrode, a Li metal reference electrode, and a Li counter electrode using CHI660D potentiostat.

***Overcharge method*:** The overcharge test was conducted in mesocarbon microbeads (MCMB)/LMO 2032 coin cells. The lamination of LMO electrode (65-75 μm thickness) was composed of 84% LMO active material, 8% super P carbon black and 8% PVDF as binder. The MCMB electrode (30-40 μm thickness) is composed of 90% MCMB active material, 2% super P carbon black and 8% PVDF binder. The celgard 2325 was used as the separator. The concentration of the BPDB was 5wt% in Gen 2 electrolyte. The cells were charged using a constant current to 200% capacity (100% overcharge ratio) or until a specific upper cutoff voltage was reached (normally 4.95V *vs.* Li/Li^+), whichever occurred first. After the charging process, the cells were discharged to a normal cutoff voltage using the same constant current.

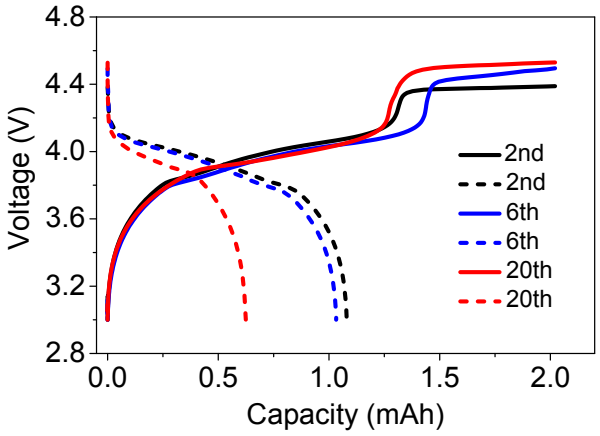

Figure S6. Voltage *vs*. capacity profiles of the LMO/MCMB cells containing 5 wt% (0.15 M) BPDB in Gen 2 electrolyte, the charging rate is C/10 and the overcharge ratio is 100%. The solid line represents the charging process while the dash line stands for discharge process.

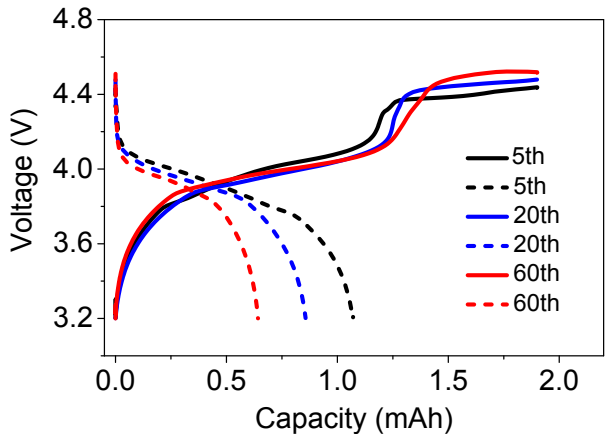

Figure S7. Voltage *vs*. capacity profiles of the LMO/MCMB cells containing 5 wt% (0.15 M) BPDB and 2 wt% (0.12 M) LiBOB in Gen 2 electrolyte, the charging rate is C/10 and the overcharge ratio is 100%.

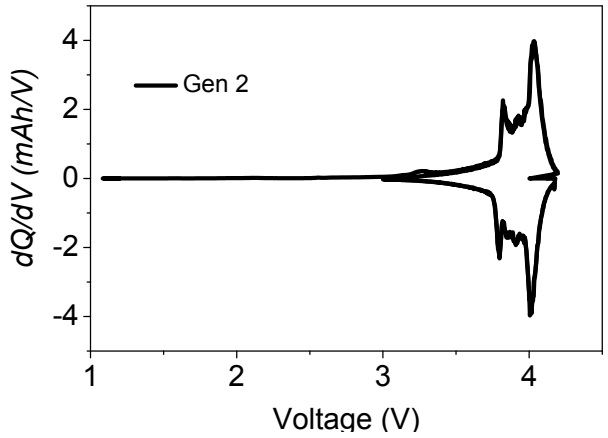

Figure S8. Differential capacity profile of the formation cycle of the cell using LMO and MCMB as electrodes and straight Gen 2 electrolyte without additive.

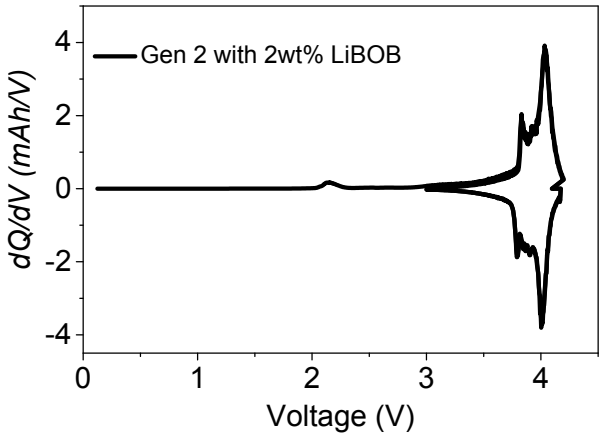

Figure S9. Differential capacity profile of the formation cycle of the cell using LMO and MCMB as electrodes and Gen 2 electrolyte with 2 wt% LiBOB.

***Scanning Electron Microscopy (SEM)*:** Scanning Electron Microscopy (SEM) examination was conducted using a high resolution Hitachi S-4700 scanning electron microscope with a field emission electron source. The samples were briefly exposed to air before insertion into the analysis chamber. The morphological changes of the electrodes were investigated.

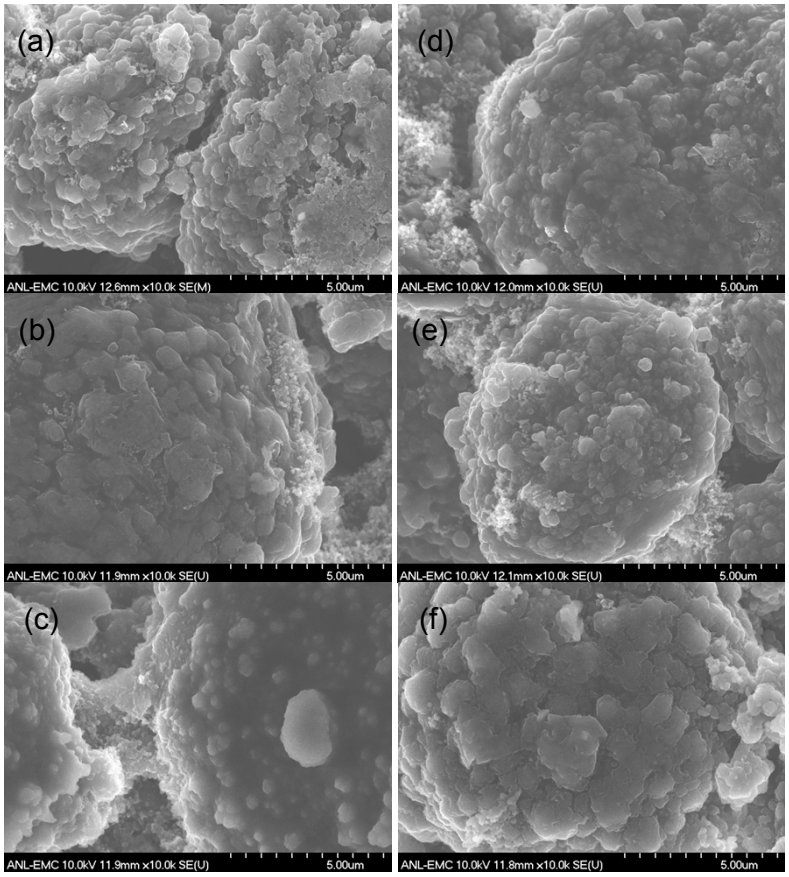

Figure S10. Scanning electron microscopy images of the harvested anodes from the cells containing (a) Gen 2 electrolyte after the 2nd formation cycle; (b) 5 wt% BPDB in Gen 2 electrolyte after the 2nd formation cycle; (c) 5 wt% BPDB in Gen 2 electrolyte after the 6th overcharge cycle; (d) 2 wt% LiBOB in Gen 2 electrolyte after the 2nd formation cycle; (e) 5 wt% BPDB and 2 wt% LiBOB in Gen 2 electrolyte after the 2nd formation cycle; (f) 5 wt% BPDB and 2 wt% LiBOB in Gen 2 electrolyte after the 6th overcharge cycle.

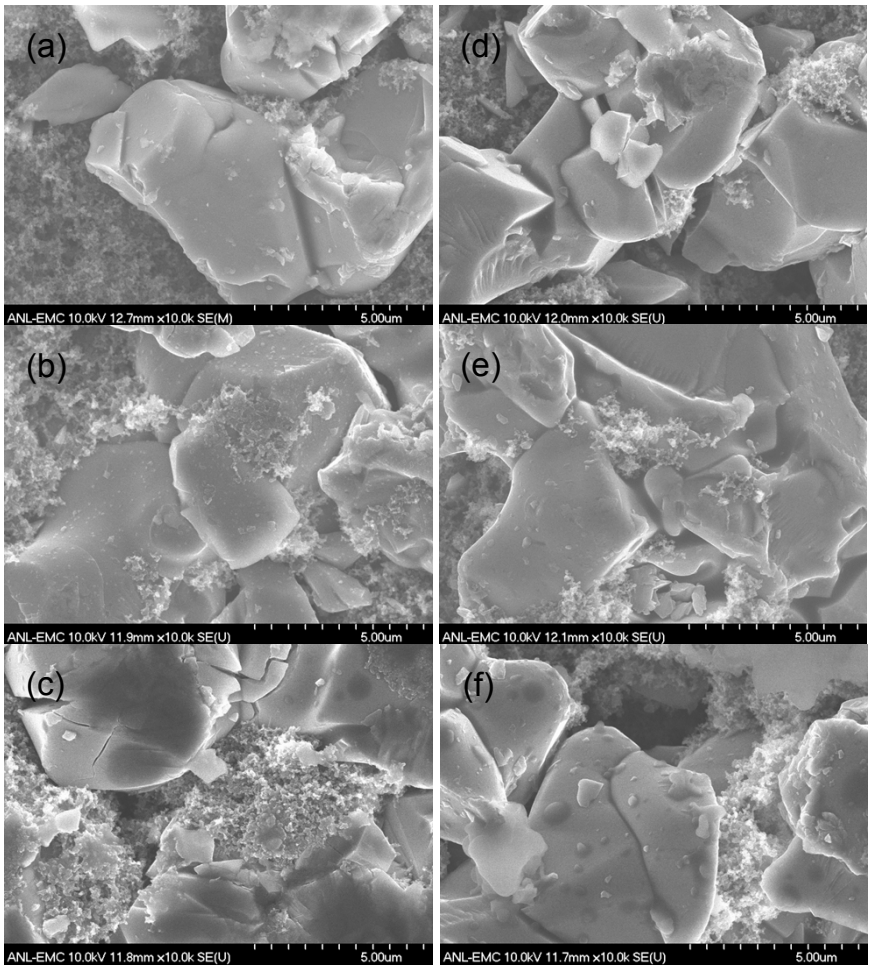

Figure S11. Scanning electron microscopy images of the harvested cathodes from the cells containing (a) Gen 2 electrolyte after the 2nd formation cycle; (b) 5 wt% BPDB in Gen 2 electrolyte after the 2nd formation cycle; (c) 5 wt% BPDB in Gen 2 electrolyte after the 6th overcharge cycle; (d) 2 wt% LiBOB in Gen 2 electrolyte after the 2nd formation cycle; (e) 5 wt% BPDB and 2 wt% LiBOB in Gen 2 electrolyte after the 2nd formation cycle; (f) 5 wt% BPDB and 2 wt% LiBOB in Gen 2 electrolyte after the 6th overcharge cycle.

Chemical reduction: The potassium metal was added to a solution of BPDB (5 mmol) in DME (5 mL) and the mixture was stirred for 30 min.

Electron Paramagnetic Resonance (EPR) measurements*:* Chemically reduced BPDB solutions were placed in glass capillaries and sealed inside of glass tubes that were subsequently transferred to the resonator of a Bruker ESP300E spectrometer that operated at the microwave frequency of 9.4347 GHz and microwave power of 2 mW. The first-derivative EPR spectra shown in Figure S12 were obtained using 0.5 G modulation at 100 kHz**.** WINSIM suite Version 0.98 (NIH) was used to analyze these EPR spectra. The magnetic field and the inferred isotropic (Fermi contact) hyperfine coupling constants (hfcc's) are given in the units of Gauss (1 G = 10^{-4} T).

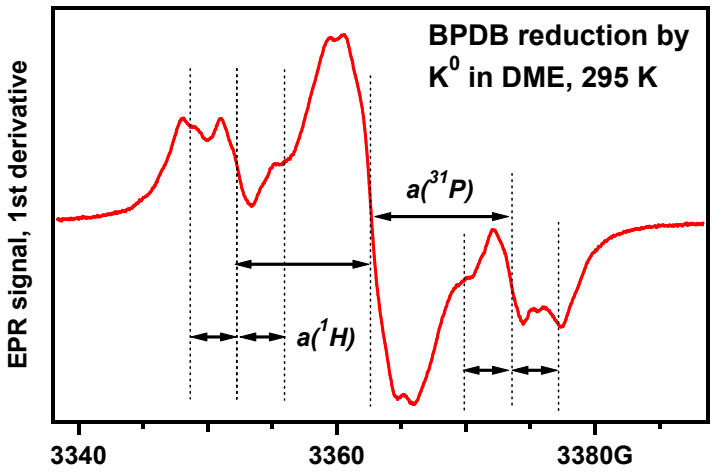

Figure S12. The first-derivative EPR spectrum of $BPDB^{-\bullet}$ anion in DME (295 K) obtained by potassium metal reduction of the parent compound in the room-temperature dimethoxyethane (DME). The center corresponds to g=2.0406. This spectrum is a triplet of triplets (as indicated with the vertical dotted lines) corresponding to two magnetically equivalent ^{31}P nuclei with the absolute hfcc's of 10.1 G and two magnetically equivalent aromatic protons with the absolute hfcc's of 2.74 G.

Our density functional theory (DFT) calculation using the B3LYP/6-31+G(d,p) method for a gas phase, C_i symmetrical radical anion of BPDB predicted negligible (< 0.5 G) hfcc's for all nuclei other than the two phosphorus-31 nuclei (estimated -11.8 G *vs*. experimental -10.1 G) and the two aromatic protons (estimated -3.4 G *vs*. experimental -2.74 G). [We remind that EPR spectroscopy does not yield the signs of the hfcc's, which were inferred from the DFT calculation]. While the radical anion clearly retains the inversion symmetry of the parent BPDB molecule, we can also conclude from the hfcc in the ^{31}P nuclei that this symmetry, in fact, must be close to the C_{2h}. Indeed, our DFT calculations indicate that in this radical anion, there is a high barrier (≈ 0.38 eV) for the rotation of the phosphine oxide group around the C_{Ar}-P bond. These calculations indicate that the hyperfine constant a for ^{31}P nuclei varies as $a(\theta)=A+B\ \sin^2(2\pi\ \theta/60^o)$ as a function of the angle θ between the aromatic ring and the P=O bond, where A=-11.8 G

and B=7.87 G; i.e., the hfcc on ^{31}P reaches the maximum negative value (A) only when the P=O bond is in the plane of the aromatic ring (θ=0), which also corresponds to the minimum energy. From this we deduce that the deviation from the planarity of the (Me)O-C-C-P=O fragment in this radical anion cannot exceed 7°.

Nuclear magnetic resonance (NMR) characterization of the reduction product. As the reduction with the metallic K proceeds further, the solution becomes murky, the parent compound progressively decays, and another species is formed, as can be demonstrated using NMR. To obtain these NMR spectra, we removed the unreacted metal, centrifuged the reaction mixture, collected the supernatant, and evaporated DME in vacuum. The residue was dissolved in $CDCl_3$, and the solution was analyzed using ^{1}H NMR.

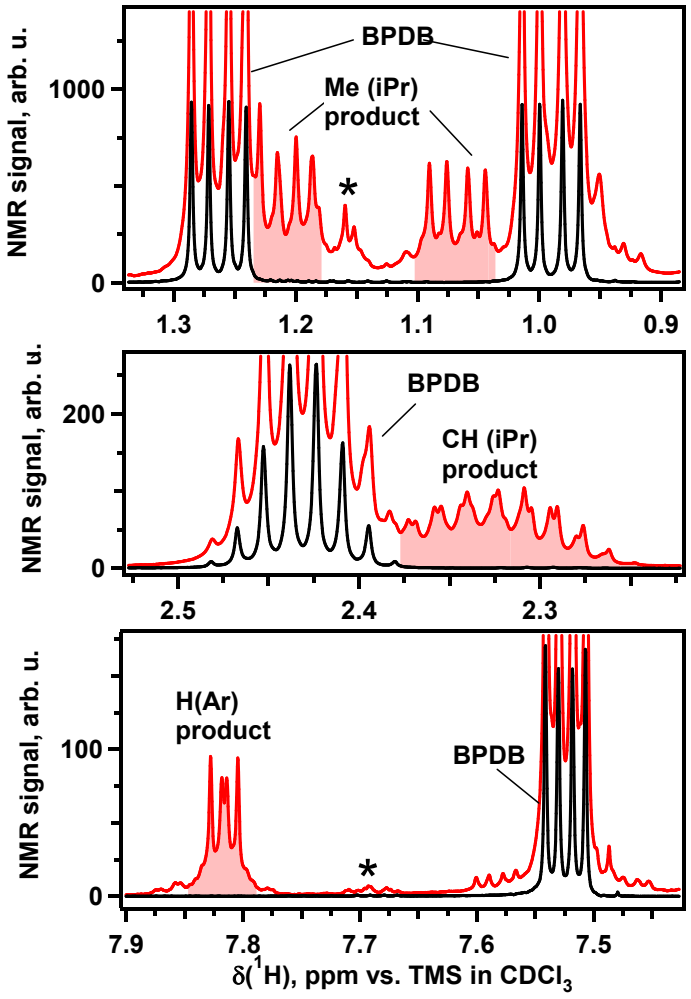

Figure S13. The ^{1}H NMR spectra (only the selected regions are shown) of BPDB before (black lines) and after the reduction with potassium in dimethoxyethane (red lines, scaled trace). The resonance lines of the main reaction product are highlighted in the plot. The asterisks indicate the impurity signals. The sidelines around the BPDB resonances are carbon-13 satellites. The chemical shifts are given vs. tetramethylsilane in $CDCl_3$.

As shown in Figure S13, while BPDB was still observed in proton NMR, some new peaks appeared after the potassium reduction, indicating a possible reductive decomposition of BPDB. The similar coupling patterns of some of the new peaks implied that the new species may have similar functional groups such as isopropyl or benzene ring.

***Crystal Structure of BPDFDB*:** Single crystal X-ray diffraction data on BPDFDB was collected on a Bruker AXS SMART three-circle diffractometer equipped with an APEX II CCD detector and Mo Kα radiation (λ=0.71073 Å). A single crystal with dimensions of 0.60 × 0.24 × 0.23 mm^3 was attached to the tip of a glass fiber and mounted on the diffractometer. Preliminary lattice parameters and orientation matrices were obtained from three sets of frames. Full data sets for structural analysis were collected with a detector distance of 50 mm. Data integration and cell refinement were performed by the SAINT program of the APEX2 software and multi-scan absorption corrections were applied using the SCALE program for area detector.[1] The structure was solved by direct methods and refined by full matrix least-squares methods on F^2. All atoms except hydrogen were refined with anisotropic thermal parameters, and the refinements converged for $I > 2\sigma(I)$. Calculations were performed using the SHELXTL crystallographic software package.[2] Details of crystal parameters, data collection and structure refinement at each temperature are summarized in Table S1. Atomic positions, anisotropic thermal parameters, selected bond distances (Å) and angles (°) are presented in Table S2-S5. Figure S14 shows the crystal structure of BPDFDB. Note that the crystal structure contains some solvent fraction.

Table S1. Crystal data and structure refinement for $C_{32}H_{62}F_2O_4P_2$ at 298K.

Empirical formula	C32 H62 F2 O4 P2
Formula weight	610.76
Temperature	298(2) K
Wavelength	0.71073 Å
Crystal system	Triclinic
Space group	P-1
Unit cell dimensions	a = 8.3768(6) Å, α = 75.782(4)° b = 9.7336(8) Å, β = 88.910(4)° c = 11.0989(9) Å, γ = 79.489(4)°
Volume	862.21(12) $Å^3$
	1
Density (calculated)	1.176 g/cm^3
Absorption coefficient	0.169 mm^{-1}
F(000)	334

Crystal size	0.60 x 0.24 x 0.23 mm^3
θ range for data collection	1.89 to 31.50°
Index ranges	-12<=h<=12, -14<=k<=14, -16<=l<=16
Reflections collected	11427
Independent reflections	5585 [R_{int} = 0.0379]
Completeness to θ = 31.50°	97%
Refinement method	Full-matrix least-squares on F^2
Data / restraints / parameters	5585 / 0 / 190
Goodness-of-fit	1.057
Final R indices [>2σ(I)]	R_{obs} = 0.0850, wR_{obs} = 0.2632
R indices [all data]	R_{all} = 0.1119, wR_{all} = 0.2964
Largest diff. peak and hole	1.001 and -0.557 e·$Å^{-3}$

$R = \Sigma||F_o|-|F_c|| / \Sigma|F_o|$, $wR = \{\Sigma[w(|F_o|^2 - |F_c|^2)^2] / \Sigma[w(|F_o|^4)]\}^{1/2}$ and calc $w=1/[\sigma^2(Fo^2)+(0.1887P)^2+0.1947P]$ where $P=(Fo^2+2Fc^2)/3$

Table S2. Atomic coordinates (x10^4) and equivalent isotropic displacement parameters ($Å^2$x10^3) for $C_{32}H_{62}F_2O_4P_2$ at 298 K with estimated standard deviations in parentheses.

Label	x	y	z	Occupancy	U_{eq}*
P(1)	4230(1)	7271(1)	2178(1)	1	38(1)
F(2)	7488(2)	9560(2)	-1517(2)	1	57(1)
O(3)	4816(2)	5884(2)	1844(2)	1	48(1)
C(4)	4655(3)	8793(3)	943(2)	1	38(1)
C(5)	5935(3)	8621(2)	137(2)	1	38(1)
C(6)	6217(3)	9804(3)	-775(2)	1	41(1)
C(7)	5214(4)	7403(3)	3567(3)	1	50(1)
H(7)	4927	6647	4251	1	61
C(8)	2048(3)	7495(3)	2421(3)	1	47(1)
H(8)	1699	8344	2752	1	56
C(9)	7321(3)	3029(3)	3731(3)	1	50(1)
H(9A)	7361	2403	4562	1	60
H(9B)	7472	3971	3802	1	60
C(10)	5765(3)	3153(3)	3147(3)	1	55(1)
H(10A)	5489	4080	2571	1	83
H(10B)	4955	3052	3770	1	83
H10C()	5813	2410	2710	1	83
C(11)	4690(5)	8817(4)	3930(3)	1	68(1)

H(11A)	4955	9591	3283	1	102
H(11B)	5243	8781	4690	1	102
H11C()	3539	8976	4047	1	102
C(3)	6603(5)	6555(3)	-627(3)	1	61(1)
H(3A)	6598	7144	-1459	1	92
H(3B)	5555	6295	-458	1	92
H3C()	7412	5697	-541	1	92
C(12)	8608(4)	2448(4)	3009(3)	1	63(1)
C(13)	1760(4)	6136(4)	3396(4)	1	67(1)
H(13A)	2178	5295	3103	1	101
H(13B)	616	6191	3528	1	101
H13C()	2306	6078	4165	1	101
C(14)	1117(4)	7682(5)	1230(4)	1	73(1)
H(14A)	1119	8630	710	1	109
H(14B)	18	7564	1413	1	109
H14C()	1619	6973	805	1	109
C(15)	8684(6)	3490(5)	1786(4)	1	80(2)
H(15A)	7690	3625	1321	1	121
H(15B)	9578	3121	1331	1	121
H15C()	8833	4397	1920	1	121
C(16)	7054(4)	7064(5)	3456(4)	1	71(1)
H(16A)	7388	6063	3469	1	107
H(16B)	7568	7271	4140	1	107
H16C()	7363	7646	2688	1	107
C(17)	8350(7)	977(5)	2833(6)	1	100(2)
H(17A)	8189	358	3627	1	150
H(17B)	9289	540	2461	1	150
H17C()	7413	1117	2302	1	150
C(18)	10058(6)	2259(6)	3850(5)	1	100(2)
H(18A)	10132	3167	4019	1	151
H(18B)	11026	1919	3452	1	151
H18C()	9944	1570	4616	1	151
O(1)	6966(2)	7340(2)	232(2)	1	45(1)

*U_{eq} is defined as one third of the trace of the orthogonalized U_{ij} tensor.

Table S3. Anisotropic displacement parameters ($Å^2x10^3$) for $C_{32}H_{62}F_2O_4P_2$ at 298 K with estimated standard deviations in parentheses.

Label	U_{11}	U_{22}	U_{33}	U_{12}	U_{13}	U_{23}
P(1)	37(1)	37(1)	38(1)	-7(1)	5(1)	-6(1)
F(2)	55(1)	45(1)	63(1)	1(1)	31(1)	-7(1)
O(3)	52(2)	38(1)	53(2)	-5(1)	8(1)	-9(1)
C(4)	38(2)	37(2)	38(2)	-5(1)	7(1)	-7(1)
C(5)	36(2)	37(2)	41(2)	-1(1)	4(1)	-9(1)
C(6)	37(2)	40(2)	43(2)	-1(1)	12(1)	-9(1)
C(7)	58(2)	54(2)	40(2)	-18(2)	0(2)	-7(2)
C(8)	37(2)	51(2)	53(2)	-10(1)	9(1)	-13(2)
C(9)	50(2)	54(2)	40(2)	-2(2)	1(1)	-5(2)
C(10)	43(2)	45(2)	66(2)	-6(2)	0(2)	6(2)
C(11)	84(2)	72(2)	57(2)	-22(2)	6(2)	-29(2)
C(3)	82(2)	45(2)	56(2)	-4(2)	15(2)	-19(2)
C(12)	59(2)	57(2)	66(2)	-3(2)	2(2)	-8(2)
C(13)	55(2)	70(2)	77(2)	-26(2)	21(2)	-8(2)
C(14)	51(2)	98(3)	68(2)	-18(2)	-9(2)	-13(2)
C(15)	89(3)	84(3)	63(2)	-18(2)	12(2)	-9(2)
C(16)	54(2)	88(3)	73(2)	-10(2)	-13(2)	-23(2)
C(17)	92(3)	63(2)	142(5)	-8(2)	-4(3)	-23(3)
C(18)	80(3)	102(3)	108(4)	-2(3)	-28(3)	-13(3)
O(1)	42(1)	36(1)	52(1)	2(1)	7(1)	-8(1)

The anisotropic displacement factor exponent takes the form: $-2\pi^2[h^2a^{*2}U_{11} + ... + 2hka^*b^*U_{12}]$.

Table S4. Bond lengths [Å] for $C_{32}H_{62}F_2O_4P_2$ at 298 K with estimated standard deviations in parentheses.

Label	Distances
P(1)-O(3)	1.4824(19)
P(1)-C(7)	1.805(3)
P(1)-C(8)	1.824(3)
P(1)-C(4)	1.838(2)
F(2)-C(6)	1.356(3)
C(4)-C(6)#1	1.396(3)
C(4)-C(5)	1.396(3)
C(5)-O(1)	1.363(3)
C(5)-C(6)	1.388(4)
C(6)-C(4)#1	1.396(3)

C(7)-C(11)	1.514(4)
C(7)-C(16)	1.525(5)
C(8)-C(14)	1.503(5)
C(8)-C(13)	1.544(4)
C(9)-C(10)	1.439(4)
C(9)-C(12)	1.447(4)
C(3)-O(1)	1.428(4)
C(12)-C(15)	1.489(5)
C(12)-C(18)	1.503(6)
C(12)-C(17)	1.545(6)

Symmetry transformations used to generate equivalent atoms:
(1) -x+1,-y+2,-z

Table S5. Bond angles [°] for $C_{32}H_{62}F_2O_4P_2$ at 298K with estimated standard deviations in parentheses.

Label	Angles
O(3)-P(1)-C(7)	113.07(13)
O(3)-P(1)-C(8)	109.77(13)
C(7)-P(1)-C(8)	108.28(14)
O(3)-P(1)-C(4)	110.81(11)
C(7)-P(1)-C(4)	105.58(12)
C(8)-P(1)-C(4)	109.19(12)
C(6)#1-C(4)-C(5)	115.5(2)
C(6)#1-C(4)-P(1)	123.06(18)
C(5)-C(4)-P(1)	121.36(18)
O(1)-C(5)-C(6)	118.0(2)
O(1)-C(5)-C(4)	122.7(2)
C(6)-C(5)-C(4)	119.3(2)
F(2)-C(6)-C(5)	116.1(2)
F(2)-C(6)-C(4)#1	118.7(2)
C(5)-C(6)-C(4)#1	125.1(2)
C(11)-C(7)-C(16)	111.0(3)
C(11)-C(7)-P(1)	115.1(2)
C(16)-C(7)-P(1)	109.9(2)
C(14)-C(8)-C(13)	111.1(3)
C(14)-C(8)-P(1)	111.4(2)
C(13)-C(8)-P(1)	106.7(2)

C(10)-C(9)-C(12)	110.3(3)
C(9)-C(12)-C(15)	109.9(3)
C(9)-C(12)-C(18)	100.9(3)
C(15)-C(12)-C(18)	113.4(4)
C(9)-C(12)-C(17)	110.5(3)
C(15)-C(12)-C(17)	111.0(4)
C(18)-C(12)-C(17)	110.7(4)
C(5)-O(1)-C(3)	114.1(2)

Symmetry transformations used to generate equivalent atoms:
(1) -x+1,-y+2,-z

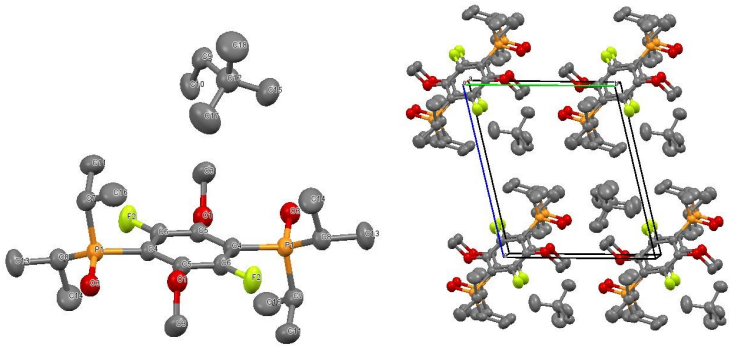

Figure S14. The crystal structure of BPDFDB. The hydrogen atoms are not shown for clarity.

(1) Bruker; Bruker Analytical X-ray Instruments, Inc.: Madison, Wisconsin, USA., 2005.
(2) Sheldrick, G. M.; version 6.12 ed.; Bruker Analytical X-ray Instruments, Inc.: Madison, WI, 2001.